High pressure investigation of an organic three-dimensional Dirac semimetal candidate having a diamond lattice

Andhika Kiswandhi,[1,*] Mitsuhiko Maesato,[1] Shinya Tomeno,[1] Yukihiro Yoshida,[1] Yasuhiro Shimizu,[2] Prashant Shahi,[3,†] Jun Gouchi,[3] Yoshiya Uwatoko,[3] Gunzi Saito,[1] and Hiroshi Kitagawa[1]

[1]*Division of Chemistry, Graduate School of Science, Kyoto University, Kitashirakawa-Oiwakecho, Sakyo-ku, Kyoto 606-8502, Japan*

[2]*Department of Physics, Nagoya University, Furo-cho, Chikusa-ku, Nagoya 464-8602, Japan*

[3]*Institute for Solid State Physics, The University of Tokyo, Kashiwanoha, Kashiwa, Chiba 277-8581, Japan*

(Received 15 February 2020; accepted 5 May 2020; published 5 June 2020)

$(ET)Ag_4(CN)_5$ [ET = BEDT-TTF: bis(ethylenedithio)tetrathiafulvalene] is a rare example of organic conductors that crystallizes in a diamond structure due to the tetrahedral arrangement of neighboring ET molecules. Because each ET has a +1 site charge, the band is half filled, which in combination with strong Coulomb interactions, turn $(ET)Ag_4(CN)_5$ into a Mott insulator. Recently, it was realized that this material may realize a nodal Dirac semimetal with a diamondlike lattice, whose state can be induced by suppressing the strong electron correlations. In this report, we present high pressure transport and optical studies on $(ET)Ag_4(CN)_5$. Our transport study indicates that the activation energy is highly suppressed by the application of hydrostatic pressure. At high pressures, the system varies from activated behavior into Coulomb gap variable range hopping.

DOI: 10.1103/PhysRevB.101.245124

I. INTRODUCTION

Dirac semimetal (DSM) state arising from linearly dispersing bands with a fourfold degenerate crossing point near the Fermi level has been attracting much attention since its discovery in the two-dimensional (2D) monolayer graphene [1,2]. Interest in DSM has been intensified by discoveries of phenomena such as large linear magnetoresistance, Fermi arc, unusual quantum oscillations, etc [3–5]. Several materials exhibiting Dirac dispersion have been discovered, such as Na_3Bi [4,6,7], Cd_3As_2 [8–11], TlBiSSe [3], a layered organic conductor α-$(ET)_2I_3$ [12,13], and a single-component molecular conductor $Pd(dddt)_2$ [14,15].

Depending on the role of symmetry, generally two classes of DSM have been recognized. In the first class, DSM occurs due to a band inversion, typically driven by spin-orbit coupling (SOC), which is symmetry protected. This mechanism results in a pairwise formation and annihilation of Dirac points. This class of DSM is realized in Na_3Bi [4,6,7] and Cd_3As_2 [8,9]. In the second type, the existence of a Dirac point is enforced only by the crystal symmetry. Here, band crossings are guaranteed to occur at certain points of high symmetry because the crossing bands belong to different irreducible representations. When such crossings occur at the Fermi level E_F, in coincidence with a vanishing density of states (DOS), the DSM state is realized [16]. In a tight-binding calculation on a diamond lattice, a band crossing can be found with a vanishing DOS at the X point of the k space, although not necessarily found at E_F [17]. In the model of Fu, Kane, and Mele considering s states and SOC, it has been shown that the crossing point at X is protected by the diamond symmetry [18]. Young *et al.* then proposed a hypothetical material β-crystobalite BiO_2 as a candidate material by considering the position of E_F and the large SOC of Bi [19]. However, although there exists a possibility for synthesizing BiO_2, it was predicted to be metastable due to the lower calculated energy and volume for the cervantite phase Bi_2O_4, implying that BiO_2 is likely difficult to obtain. So far, diamond lattice DSM has not yet been realized experimentally.

Our material of interest, $(ET)Ag_4(CN)_5$ [20], belongs to the family of organic conductors with ET as the building block. $(ET)Ag_4(CN)_5$ crystallizes in an orthorhombic ($Fddd$) structure with the lattice parameters given by $a = 13.2150(9)$Å, $b = 19.4783(13)$Å, and $c = 19.6506(13)$Å [Fig. 1(a)] [21]. Each ET in $(ET)Ag_4(CN)_5$ exists as a monocationic ET^+, which is arranged tetrahedrally to its nearest neighboring ET^+ [Fig. 1(b)] and interacting via a pair of S-S contact (3.91 Å). The diamond geometry character of $(ET)Ag_4(CN)_5$ is justified by the equal transfer integral between two nearest neighboring ET molecules, $t_{1-2} = t_{1-3} = t_{1-4} = t_{1-5} = -68.442$ meV [21,22]. $(ET)Ag_4(CN)_5$ is unique among organic conducting salts because it possesses a three-dimensional donor network, resulting from its honeycomblike anion opening formed by $[Ag_4(CN)_5^-]_\infty$ chain, which is large enough to accommodate an ET molecule [20]. Within the polyanion, C/N disorder exists in the bridging CN along the c-axis [Fig. 1(c)].

$(ET)Ag_4(CN)_5$ was initially predicted to be a semimetal [20,23]. However, its regular arrangement of donor and anion and the half-filled band should result in a Mott insulating state if the electron correlation is strong enough. Recent studies

*kiswandhi@issp.u-tokyo.ac.jp; Present address: Institute for Solid State Physics, The University of Tokyo, Kashiwanoha, Kashiwa, Chiba 277-8581, Japan.

†Present address: Department of Physics, D.D.U. Gorakhpur University, Gorakhpur 273009, India.

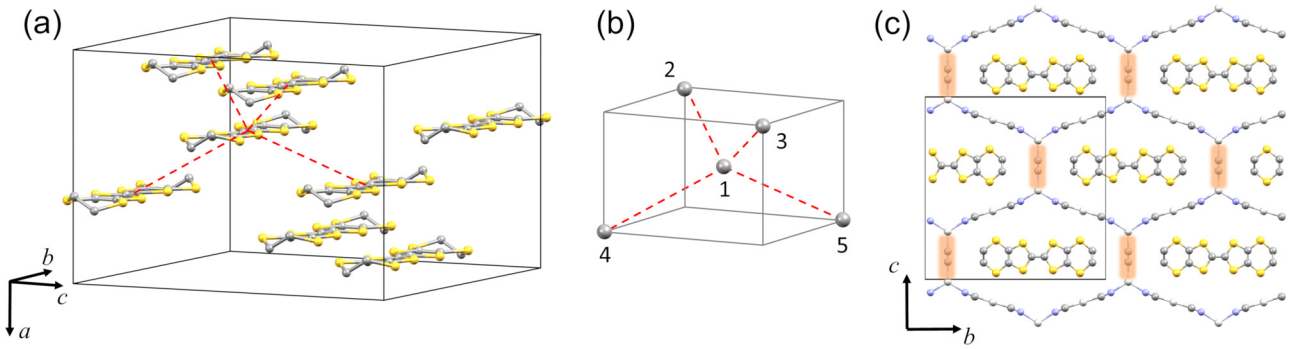

FIG. 1. Structure of (ET)$Ag_4(CN)_5$. (a) Tetrahedral arrangement of neighboring ET molecules (red dashed line) in a unit cell of (ET)$Ag_4(CN)_5$ (anion is not shown). (b) The orientation of the tetrahedrally arranged ET molecules shown in panel (a). (c) (ET)$Ag_4(CN)_5$ viewed along the a axis, showing ET molecules positioned inside a honeycomblike network of $[Ag_4(CN)_5^-]_\infty$ chain. The highlighted part of the anion denotes disordered C/N in the direction $\parallel c$.

confirmed that (ET)$Ag_4(CN)_5$ is indeed a Mott insulator (effective on-site Coulomb interaction $U_{\text{eff}} = 0.71$–0.78 eV $>$ bandwidth $W = 0.57$ eV) with an antiferromagnetic transition at $T_N = 102$ K at ambient pressure [21,22]. Under a high pressure of 2 GPa, T_N can be significantly increased to 195 K, the highest T_N so far among molecular materials. Moreover, the band structure reveals a Dirac-like dispersion near the Fermi level with a linearly vanishing DOS, $g(E) \propto E - E_F$, consistent with the characteristics of a diamond lattice [17]. Since ET contains only relatively light elements and the ET molecular planes in (ET)$Ag_4(CN)_5$ are parallel to each other, the SOC is expected to be low [24]. Therefore, this system may potentially provide a platform to study the transition from a Mott insulating state to a three-dimensional (3D) DSM state in the small SOC regime [25].

In this paper, we investigate the possibility of inducing a Dirac semimetal phase in (ET)$Ag_4(CN)_5$. The electronic properties were characterized using transport and Raman measurements under high pressures up to 14 and 3.1 GPa, respectively. The conduction mechanism follows Coulomb gap variable range hopping (VRH) mechanism and a power law behavior $\rho \propto T^{-\alpha}$ at high pressure, indicating a proximity to the closure of the activation gap.

II. EXPERIMENTAL

Single crystals of (ET)$Ag_4(CN)_5$ were synthesized by an electrocrystallization method following the procedures by Hiramatsu *et al.* [26]. Other phases, such as κ-$(ET)_2Ag_2(CN)_3$, α'-$(ET)_2Ag(CN)_2$, and κ-$(ET)_2Ag(CN)_2{\cdot}H_2O$ were manually separated under an optical microscope according to their colors and morphologies.

Standard four-probe dc transport measurements under high pressure were performed by using a BeCu-NiCrAl double layer clamp-type cell for a pressure range up to 3 GPa and a cubic anvil cell for higher pressures up to 14 GPa. In the clamp-cell measurement, a manganin wire was used as a pressure gauge. For the cubic anvil measurement, the applied pressure was obtained from the load applied by the press by a conversion following a pressure-load calibration based on the phase transition of Bi metal and lead. Electrical contacts were made by attaching gold wires to the sample with carbon paint. The sample was then coated with a thin layer of enamel to prevent the wires from detaching during measurements. All high pressure experiments were performed by using Daphne oil 7474 [27] as the pressure medium for consistency.

Raman spectroscopy measurements were carried out using a JASCO NRS-5000 spectrometer equipped with a polarized He-Ne source (632.8 nm). For high pressure measurements, a miniature diamond anvil cell was used. The pressure was measured by using the shift of the fluorescence peak of a ruby piece included in the sample space. Sample irradiation was performed with incident light polarized parallel to the b axis on the ab plane.

III. RESULTS

A. Transport measurements at P $\leqslant$ 3.1 GPa

Figures 2(a) and 2(b) show the temperature dependence of the resistivity at high pressures up to 3.1 GPa. The data for 2.41 and 2.91 GPa are plotted separately in Fig. 2(b) for clarity. At ambient pressure (ET)$Ag_4(CN)_5$ is a semiconductor with a resistivity $\rho \approx 180$ Ωcm and an activation energy $E_a \approx 1700$ K in the ab plane, consistent with the report by Shimizu *et al.*, which is attributed to the Mott insulating state [21]. All of the data were fitted to Arrhenius activation model in a temperature range between 220 and 300 K. As shown in Fig. 2(c), both ρ and E_a initially show a monotonic decrease, followed by an abrupt increase at $P' \approx 2.2$ GPa, which indicates a transition, before decreasing again above P'. All of the $\ln\rho$ vs $1/T$ curves, except at 2.91 GPa, show an upward bend below approximately 200 K. Extrapolation of E_a to zero indicates that the semiconducting state could be completely suppressed at approximately 5 GPa as shown by the dashed line in Fig. 2(c).

B. Raman measurements at $P \leqslant 3.1$ GPa

We then investigated the charge state of ET by examining the charge sensitive Raman peaks ν_2 and ν_3 [28,29]. As shown in Fig. 3(a), at ambient pressure, ν_3 peak appears as the strongest peak at 1420.3 cm^{-1}, while ν_2 peak appears well separated at 1459.2 cm^{-1}. The site charge of ET was calculated from the locations of the peaks following

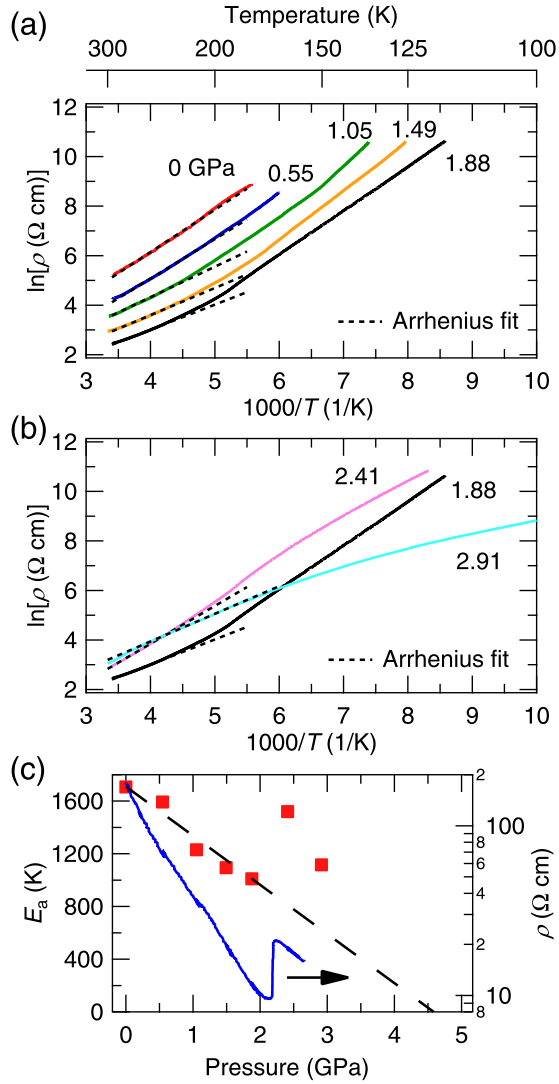

FIG. 2. Transport properties of $(ET)Ag_4(CN)_5$ under high pressures. (a) Temperature dependence of resistivity represented as $\ln\rho$ vs $1/T$ for $P < P'$ and (b) for $P > P'$. For panels (a) and (b), a temperature scale is given at the top for a reference. In (b), the resistivity at $P = 1.88$ GPa is included as a reference. The dashed lines are fits to the Arrhenius activated behavior. (c) Pressure dependence of the activation energy (left axis) and the resistivity at room temperature (right axis) showing a sudden resistivity jump at $P' \approx 2.2$ GPa.

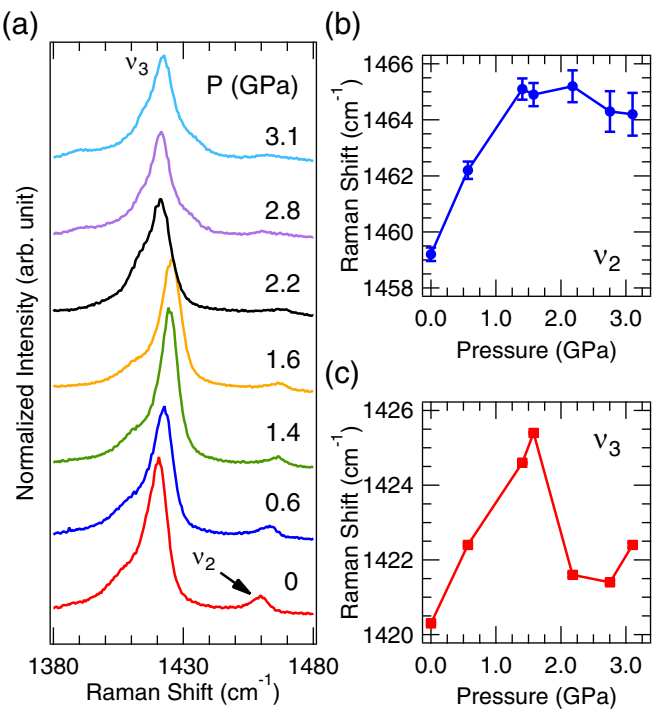

FIG. 3. (a) Raman spectra taken under different pressures. (b) Pressure dependence of the position of the ν_2 peak. (c) Pressure dependence of the position of the ν_3 peak. The data show a sudden shift of the ν_3 peak at $P \approx 2.2$ GPa indicating a transition.

the equations by Wang *et al.* [28] for the ν_3 peak and by Yamamoto *et al.* [29] for the ν_2 peak, which are valid for ET at ambient pressure. The resulting ambient pressure site charge calculated from both peaks indicate a site charge close to $+1$ ($+0.90$ by using the ν_2 peak and $+0.99$ by using the ν_3 peak). Therefore, ET in $(ET)Ag_4(CN)_5$ exists as a fully ionized ET^+ monomer. As shown in Figs. 3(b) and 3(c), as the pressure is increased, both peak initially shift towards higher wave numbers, which is expected due to a higher vibrational energy in the compressed molecule. At P', however, ν_3 shifts abruptly towards a lower wave number, indicating a transition. However, no peak splitting was observed in any of the peaks before and after the transition. This indicates that the $+1$ state of ET is maintained, thus the transition is likely a structural transition.

C. Transport measurements using a cubic anvil cell

The transport measurement data obtained using the cubic anvil cell [Fig. 4(a)] show that $(ET)Ag_4(CN)_5$ remains semiconducting at all pressures $\leqslant 14$ GPa. We first discuss the fitting for resistivity data presented in Figs. 4(b) and 4(c). The 1 GPa and 2 GPa data were fitted to Arrhenius conduction in a temperature range of 220 K $\leqslant T \leqslant$ 300 K. The resulting activation energies are in a good agreement with those obtained with the clamp-cell. At $P \geqslant 4$ GPa, $\ln\rho$ vs $1/T$ curves show a downward bend below approximately 200 K, similar to the clamp-cell data at 2.91 GPa. Unlike any results obtained at lower pressures, at $P \geqslant 4$ GPa we found the linear part of $\ln\rho$ vs $1/T$ at temperatures lower than 180 K. Hence, we separated the temperature regions for analysis into a high temperature (HT) region above 180 K and a low temperature (LT) region below 180 K. The calculated E_a in the HT region was found to be relatively insensitive to pressure, so we considered only the transport mechanism in the LT region. As the pressure increases, the linear part of the $\ln\rho$ vs $1/T$ curve shifts towards lower temperatures and spans a narrower temperature range. Finally, at 14 GPa, no linear region could be found. This behavior indicates that the conduction mechanism gradually becomes non-Arrhenius with increasing pressure. For clarity, we provide a schematic summarizing all of the fitting regions for $P \geqslant 4$ GPa in Fig. 5(d). Figure 4(d) shows the result of the Arrhenius fit to the resistivity data, which indicates a

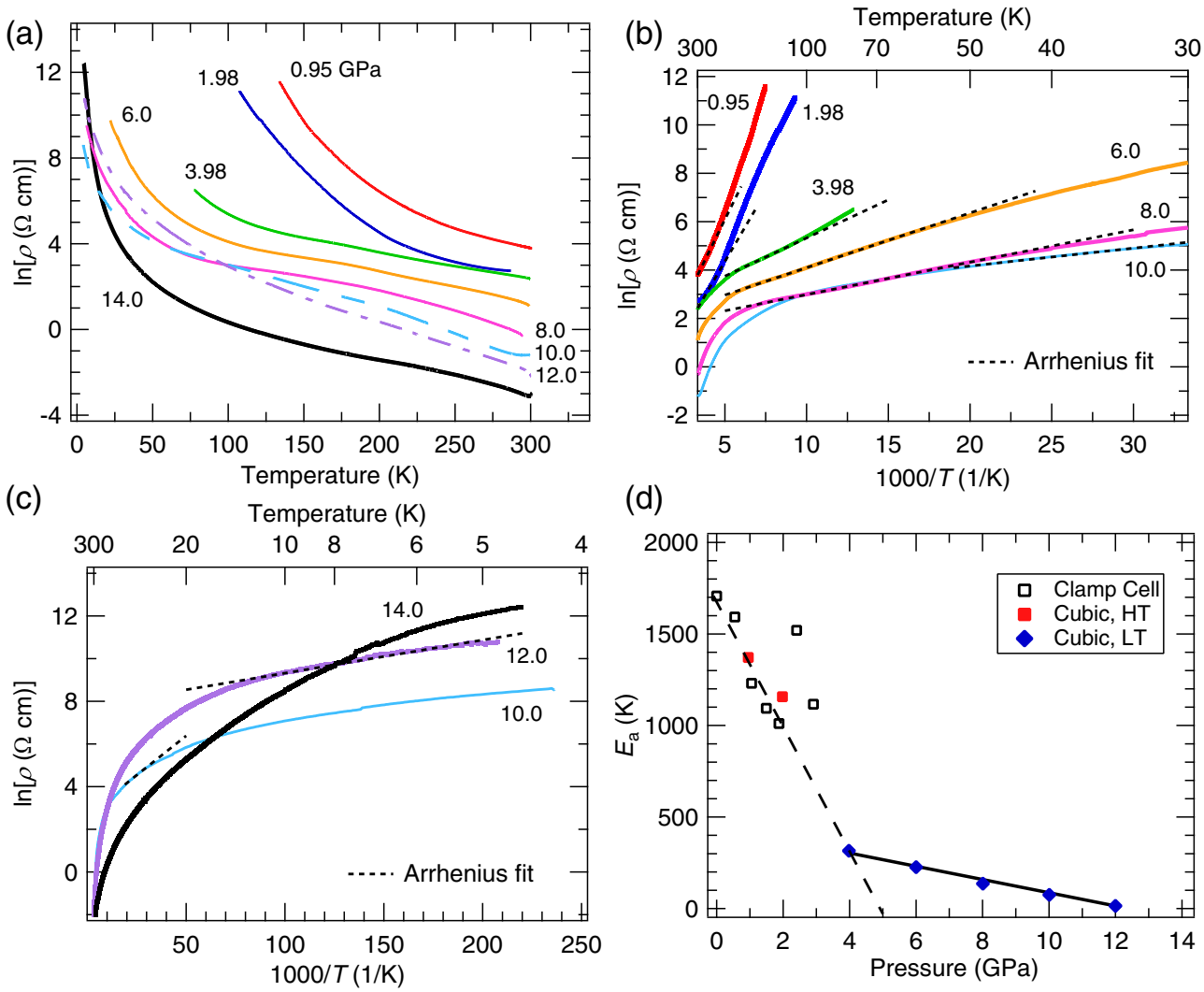

FIG. 4. Resistivity data measured under different pressures in the cubic anvil cell. (a) Resistivity as a function of temperature under different pressures (b) $\ln\rho$ vs $1/T$ representation of resistivity data for $P \leqslant 10$ GPa and (c) for $P \geqslant 10$ GPa. The dashed lines are fits to Arrhenius equation. (d) Pressure dependence of E_a. HT and LT denote the high temperature and the low temperature regions described in the text. The solid line is just a guide to the eye.

narrowing gap with increasing pressure. However, there is no indication of a finite resistivity at zero temperature.

The transport behavior at $P \geqslant 8$ GPa indicates a crossover between an activated and a VRH-like behavior [Fig. 5(a)], with a possible power-law behavior [Fig. 5(b)]. At 8 GPa, the activated behavior was found in a limited temperature range from 60 to 108 K. At lower temperatures between $T =$ 10 and 40 K, fitting to a power law $\rho(T) \propto T^{-\alpha}$ with $\alpha =$ 2.66 is possible. A VRH-like behavior $\rho = \rho_0 \exp((T_0/T)^{1/2})$ was observed below 10 K. Interestingly, the temperature dependent resistivity at 10 GPa can be described by a power law behavior, with a lower $\alpha = 1.78$, over a wide range of temperature (6 K—120 K). At $P = 12$ GPa, the room temperature resistivity is lowered, but the resistivity at $T <$ 95 K becomes higher than the resistivity at 10 GPa in the same temperature range. At 14 GPa, the room temperature resistivity is suppressed further, but the resistivity at low temperatures shows a steeper increase with decreasing temperature (higher E_a) compared with that at 12 GPa. This behavior suggests that a localization effect is present at low T, high P region.

IV. DISCUSSION

In Mott insulators, a decrease in E_a following a pressure increase can be understood as a consequence of the broadening of Hubbard bands, closing the charge gap. Because $T_N \propto J \propto t^2/U$, the band broadening due to increasing pressure is consistent with the increase of T_N in $(ET)Ag_4(CN)_5$ reported by Shimizu *et al.* [21]. In compensated semiconductors near a metal-insulator transition, power law $T^{-\alpha}$ behavior has been observed, with decreasing α as the transition is approached from the insulating phase [30,31]. In Weyl and Dirac semimetals ($E_a = 0$), $\rho(T)$ is described only by a power law [32–34] with α depending on the details of disorder, screening, electron-phonon scattering, and DOS. For a 3D DSM with a linear dispersion, $\alpha = 0$ or 4 [33,34] or 1 [15]

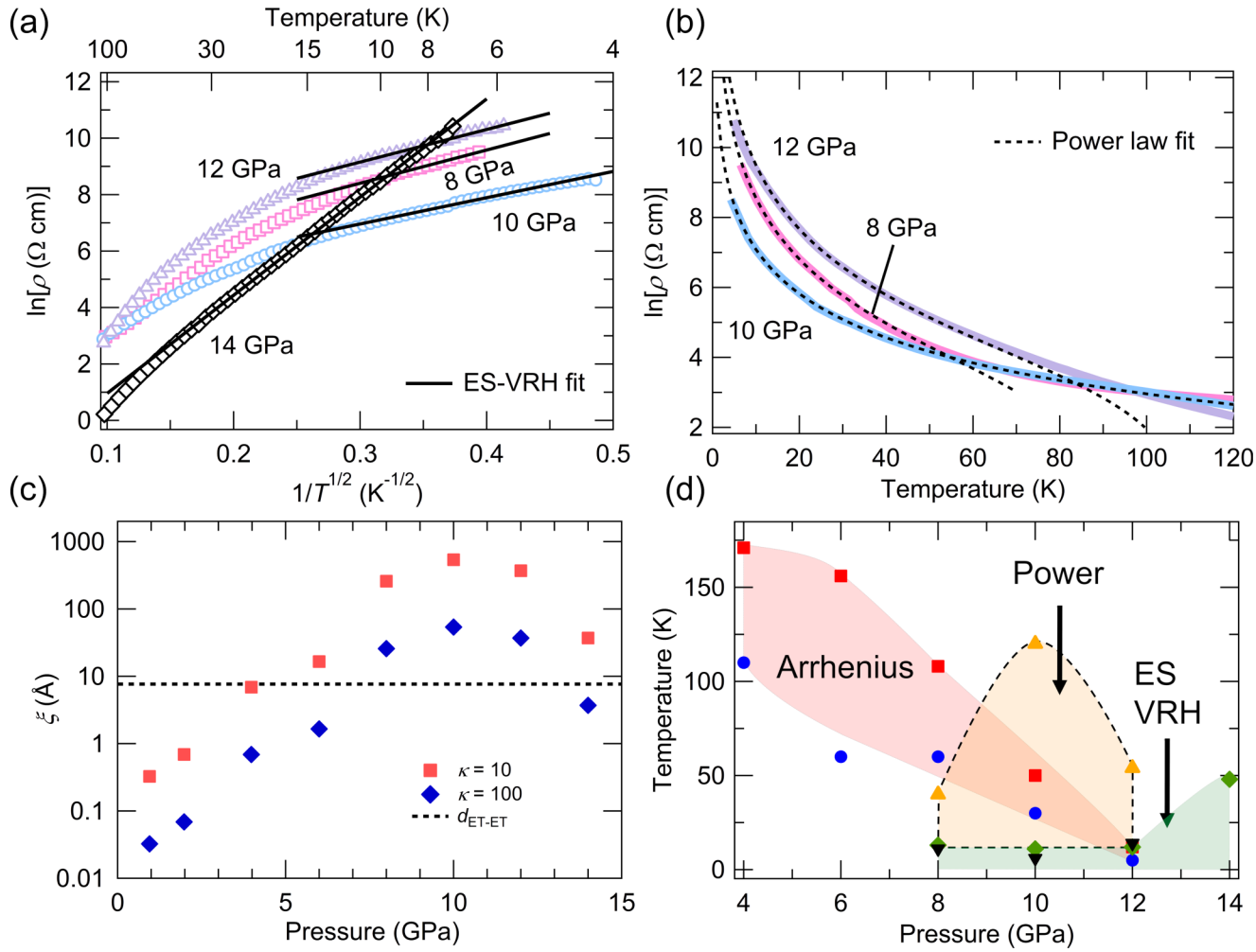

FIG. 5. Non-Arrhenius transport mechanisms found at LT. (a) $\ln\rho$ vs $T^{-1/2}$ representation of resistivity. The solid lines are fits to the ES-VRH model. (b) $\ln\rho$ vs T representation of resistivity. The dashed curves are fitting results to the power function described in the text. (c) ES-VRH localization length extracted using Eq. (2). The symbols correspond to the localization lengths obtained by assuming $\kappa = 10$ (squares) and $\kappa = 100$ (diamonds). The dotted line is $d_{\text{ET-ET}}$ at ambient pressure as a reference. (d) Schematic diagram summarizing the T-P regions where Arrhenius (red), ES-VRH (green) and power law (yellow) fits were performed. Symbols denote the temperature limits of the fits: squares and circles are the upper and the lower temperature limits of Arrhenius fit, respectively; diamonds are the upper temperature limit of the ES-VRH fit; triangles and inverted triangles denote the upper and lower temperature limits for the power-law fit. ES-VRH fit at each pressure was performed down to the lowest measurable temperature. Unshaded regions are regions where no fitting could be performed.

were suggested. In the present case with $(ET)Ag_4(CN)_5$, α decreases with increasing P from 8 GPa to 10 GPa. However, neither of the aforementioned α is observed. It is possible that the system becomes a disordered Mott or a correlated Anderson insulator, close to a semimetallic phase, as suggested by the presence of the VRH-type conduction at low temperatures and high pressures.

In general, a VRH conduction is described by

$$\rho(T) = \rho_0 \exp((T_0/T)^{\beta}), \tag{1}$$

which is commonly observed at low temperatures in systems with low carrier densities and dominating disorder. Here, β is given by $1/(1+d)$, where d is the dimensionality of the system. The value of $\beta = 1/2$ is also associated with the Efros-Skhlovskii variable range hopping (ES-VRH) mechanism, regardless of the dimensionality [35]. The ES-VRH model accounts for the electron-hole Coulomb interactions arising from the hopping of an electron from one site to another. As the temperature is lowered, the system cannot provide a sufficient energy to overcome this interaction, resulting in a vanishing DOS near the Fermi level. In the ES-VRH model, the DOS near the Fermi level vanishes as $g(E) \propto E - E_F$ and $g(E) \propto (E - E_F)^2$ for 2D and 3D systems, respectively. The ES-VRH model is consistent with the large Coulomb interactions present in $(ET)Ag_4(CN)_5$. From the ES-VRH fitting to the resistivity data, we estimated the localization length ξ as given by

$$\xi = 2.8e^2/4\pi\kappa\epsilon_0 k_B T_0, \tag{2}$$

where e, κ, ϵ_0, and T_0 are the electron charge, the dielectric constant, the permittivity in vacuum, and the characteristic temperature in the ES-VRH model, respectively. Assuming dielectric constant values between 10 and 100 as the lower and upper limits, which covers a wide range of molecular

materials [36], our estimation shows that above 6 GPa, ξ is larger than the distance between the nearest neighboring ET molecules $d_{\text{ET-ET}}$ at ambient pressure [Fig. 5(c)]. In the VRH conduction model, ξ is defined as the extent of the wavelength of a localized electron that is not exponentially small [37]. The hopping electrons should originate from the ET sites, thus $\xi > d_{\text{ET-ET}}$ means that it is possible for the electrons to hop from an ET molecule to another within the localization length. Therefore, the ES-VRH model can explain the low temperature transport behavior of $(ET)Ag_4(CN)_5$ at high pressures.

Generally, a transition into a metallic phase may pass through a nontrivial phase due to a vanishingly small energy gap and/or disorder, including phase coexistence/separation, which can be observed in systems near a first-order transition [38,39]. As an example, $Ca_{2-x}Sr_xRuO_4$ [39], a disordered 2D Mott insulator, shows changes in its conduction behavior near the insulator-metal transition point. In the insulating phase it shows an ES-VRH like conduction, but its $\xi \approx 0.03$Å is smaller than its Ru-Ru interatomic distance. It was proposed that the VRH-like mechanism arises from electrons, which are localized in the overlapping tails of the upper and the lower Hubbard bands, with a disorder-modified DOS near E_F being the main factor for the $\beta = 1/2$ dependence. In our case, ξ is higher than the distance between ET molecules, making the phase separation scenario unlikely. However, the ES-VRH behavior is indicative of the presence of a certain disorder in $(ET)Ag_4(CN)_5$.

In the case of a half-filled honeycomb lattice, it has been shown that disorder can induce a localization of Dirac electrons, where the system enters a correlated Anderson phase or a disordered Mott insulating phase [40]. In ET-based organic conductors with C/N disorder in the anion layers, such as κ-$(ET)_2Cu_2(CN)_3$ and κ-$(ET)_2Ag_2(CN)_3$, the effects of the C/N disorder on the transport properties have been studied [41,42]. It was proposed that the C/N disorder induces disorder in ET molecules via the hydrogen bonds between the ethylene group at the tails of ET and the CN group of the anion. In $(ET)Ag_4(CN)_5$, the hydrogen atoms of the ethylene group of ET are also located near the disordered CN of the anion. Therefore, the same scenario may also occur, resulting in VRH behavior. The observed ES-VRH type can be a consequence of disorder, strong Coulomb interactions, and a vanishing DOS near the Fermi level due to the diamond symmetry.

We also would like to point out the possibility of transition into a topological insulator. The standard model for half-filled organic conductors with strong Coulomb interactions predicts that monomeric phases must exist as Mott insulators [43], which is observed in $(ET)Ag_4(CN)_5$ at ambient pressure. Although structural determination under high pressure is ongoing, if a structural transition occurs and the symmetry is lowered, the system can be regarded as a nonmagnetic band insulating state due to Peierls distortion and ET^+ will be dimerized. As a half-filled Mott insulator, the next nearest neighbor Coulomb interaction V is likely small compared with U. The strength of SOC must then be considered. In the context of strongly dimerized ET materials, SOC strength depends on the relative orientation of the two ET molecular planes within a dimer. The SOC is the strongest when the two ET planes are oriented perpendicular to each other [24]. In $(ET)Ag_4(CN)_5$, the ET planes are all parallel to each other, so the SOC should be small. In the presence of a strong U and a weak SOC the dimerized system can undergo a transition into a semimetal phase [25]. However, if the SOC is significant, it can induce a band inversion in the bulk as the semimetallic phase is approached, resulting in a strong topological insulator phase under high pressure [18].

In summary, the dc transport properties of an organic DSM candidate with a diamond symmetry in the presence of strong Coulomb interactions and disorder have been studied. The result shows that the electron correlation in $(ET)Ag_4(CN)_5$ is reduced by increasing pressure. A transition occurs at $P = 2.2$ GPa that appears in the transport behavior, but does not affect the charge state of ET. The conduction at high pressures and low temperatures can be explained by ES-VRH due to the presence of disorder, Coulomb interactions, and a vanishing DOS. At 10 GPa, the low temperature conduction of $(ET)Ag_4(CN)_5$ can be described as $\rho \propto T^{-\alpha}$, indicating a proximity to an insulator-metal transition, possibly semimetallic behavior.

ACKNOWLEDGMENTS

We thank Y. Nakamura and H. Kishida for helpful discussions. A.K. thanks JSPS Postdoctoral Fellowships for Research in Japan (Grant No. P17041). This work was supported by a Grant-in-Aid for Scientific Research from JSPS KAKENHI, Grant No. JP23225005 "Development of multi-electronic-functions based on spin triangular lattice" and a Grant-in-Aid for JSPS Fellows, Grant No. JP17F17041. Y.S. was supported by JSPS KAKENHI, Grant No. JP19H05824, the work at ISSP and Y.U. were supported in part by Grant No. JP19H00648, and P.S. by DST-SERB Project No. SRG/2019/001187.

[1] K. S. Novoselov, A. K. Geim, S. V. Morozov, D. Jiang, Y. Zhang, S. V. Dubonos, I. V. Grigorieva, and A. A. Firsov, Science **306**, 666 (2004).

[2] K. S. Novoselov, A. K. Geim, S. V. Morozov, D. Jiang, M. I. Katsnelson, I. V. Grigorieva, S. V. Dubonos, and A. A. Firsov, Nature (London) **438**, 197 (2005).

[3] M. Novak, S. Sasaki, K. Segawa, and Y. Ando, Phys. Rev. B **91**, 041203(R) (2015).

[4] S.-Y. Xu, C. Liu, S. K. Kushwaha, R. Sankar, J. W. Krizan, I. Belopolski, M. Neupane, G. Bian, N. Alidoust, T.-R. Chang, H.-T. Jeng, C.-Y. Huang, W.-F. Tsai, H. Lin, P. P. Shibayev, F.-C. Chou, R. J. Cava, and M. Z. Hasan, Science **347**, 294 (2015).

[5] X. Wan, A. M. Turner, A. Vishwanath, and S. Y. Savrasov, Phys. Rev. B **83**, 205101 (2011).

[6] Z. K. Liu, B. Zhou, Y. Zhang, Z. J. Wang, H. M. Meng, D. Prabhakaran, S.-K. Mo, Z. X. Shen, Z. Fang, X. Dai, Z. Hussain, and Y. L. Chen, Science **343**, 864 (2014).

[7] Z. Wang, Y. Sun, X.-Q. Chen, C. Franchini, G. Xu, H. Weng, X. Dai, and Z. Fang, Phys. Rev. B **85**, 195320 (2012).

[8] Z. Wang, H. Weng, Q. Wu, X. Dai, and Z. Fang, Phys. Rev. B **88**, 125427 (2013).

[9] Z. K. Liu, J. Jiang, B. Zhou, Z. J. Wang, Y. Zhang, H. M. Weng, D. Prabhakaran, S.-K. Mo, H. Peng, P. Dudin, T. Kim, M. Hoesch, Z. Fang, X. Dai, Z. X. Shen, D. L. Feng, Z. Hussain, and Y. L. Chen, Nat. Mater. **13**, 677 (2014).

[10] M. Neupane, S.-Y. Xu, R. Sankar, N. Alidoust, G. Bian, C. Liu, I. Belopolski, T.-R. Chang, H.-T. Jeng, H. Lin, A. Bansil, F. Chou, and M. Z. Hasan, Nat. Commun. **5**, 3786 (2014).

[11] S. Borisenko, Q. Gibson, D. Evtushinsky, V. Zabolotnyy, B. Büchner, and R. J. Cava, Phys. Rev. Lett. **113**, 027603 (2014).

[12] N. Tajima, S. Sugawara, M. Tamura, R. Kato, Y. Nishio, and K. Kajita, Europhys. Lett. **80**, 47002 (2007).

[13] K. Kajita, Y. Nishio, N. Tajima, Y. Suzumura, and A. Kobayashi, J. Phys. Soc. Jpn. **83**, 072002 (2014).

[14] R. Kato, H. Cui, T. Tsumuraya, T. Miyazaki, and Y. Suzumura, J. Am. Chem. Soc. **139**, 1770 (2017).

[15] Y. Suzumura, H. Cui, and R. Kato, J. Phys. Soc. Jpn. **87**, 084702 (2018).

[16] Q. D. Gibson, L. M. Schoop, L. Muechler, L. S. Xie, M. Hirschberger, N. P. Ong, R. Car, and R. J. Cava, Phys. Rev. B **91**, 205128 (2015).

[17] D. J. Chadi and M. L. Cohen, Phys. Status Solidi B **68**, 405 (1975).

[18] L. Fu, C. L. Kane, and E. J. Mele, Phys. Rev. Lett. **98**, 106803 (2007).

[19] S. M. Young, S. Zaheer, J. C. Y. Teo, C. L. Kane, E. J. Mele, and A. M. Rappe, Phys. Rev. Lett. **108**, 140405 (2012).

[20] U. Geiser, H. H. Wang, L. E. Gerdom, M. A. Firestone, L. M. Sowa, and J. M. Williams, J. Am. Chem. Soc. **107**, 8305 (1985).

[21] Y. Shimizu, A. Otsuka, M. Maesato, M. Tsuchiizu, A. Nakao, H. Yamochi, T. Hiramatsu, Y. Yoshida, and G. Saito, Phys. Rev. B **99**, 174417 (2019).

[22] A. Otsuka, Y. Shimizu, G. Saito, M. Maesato, A. Kiswandhi, T. Hiramatsu, Y. Yoshida, H. Yamochi, M. Tsuchiizu, Y. Nakamura, H. Kishida, and H. Ito, Bull. Chem. Soc. Jpn. **93**, 260 (2020).

[23] U. Geiser, H. H. Wang, and J. M. Williams, E. L. Venturini, J. F. Kwak, and M.-H. Whangbo, Synth. Met. **19**, 599 (1987).

[24] S. M. Winter, K. Riedl, and R. Valentí, Phys. Rev. B **95**, 060404(R) (2017).

[25] Y. Zhang, Y. Ran, and A. Vishwanath, Phys. Rev. B **79**, 245331 (2009).

[26] T. Hiramatsu, Y. Yoshida, G. Saito, A. Otsuka, H. Yamochi, M. Maesato, Y. Shimizu, H. Ito, Y. Nakamura, H. Kishida, M. Watanabe, and R. Kumai, Bull. Chem. Soc. Jpn. **90**, 1073 (2017).

[27] K. Murata, K. Yokogawa, H. Yoshino, S. Klotz, P. Munsch, A. Irizawa, M. Nishiyama, K. Iizuka, T. Nanba, T. Okada, Y. Shiraga, and S. Aoyama, Rev. Sci. Instrum. **79**, 085101 (2008).

[28] H. H. Wang, J. R. Ferraro, J. M. Williams, U. Geiser, and J. A. Schlueter, J. Chem. Soc., Chem. Commun. 1893 (1994), doi: 10.1039/C39940001893.

[29] T. Yamamoto, M Uruichi, K. Yamamoto, K. Yakushi, A. Kawamoto, and H. Taniguchi, J. Phys. Chem. B **109**, 15226 (2005).

[30] A. G. Zabrodskii and K. N. Zinov'eva, Sov. Phys. JETP **59**, 425 (1984).

[31] A. G. Zabrodskii, A. G. Andreev, and S. V. Egorov, Phys. Status Solidi B **205**, 61 (1998).

[32] P. Hosur, S. A. Parameswaran, and A. Vishwanath, Phys. Rev. Lett. **108**, 046602 (2012).

[33] S. Das Sarma, E. H. Hwang, and H. Min, Phys. Rev. B **91**, 035201 (2015).

[34] S. Das Sarma and E. H. Hwang, Phys. Rev. B **91**, 195104 (2015).

[35] A. L. Efros and B. I. Shklovskii, J. Phys. C **8**, L49 (1975).

[36] K. Sano, T. Sasaki, N. Yoneyama, and N. Kobayashi, Phys. Rev. Lett. **104**, 217003 (2010).

[37] B. I. Shklovskii and A. L. Efros, *Electronic Properties of Doped Semiconductors* (Springer-Verlag, Berlin, 1984).

[38] E. Dagotto, T. Hotta, and A. Moreo, Phys. Rep. **344**, 1 (2001).

[39] S. Nakatsuji, V. Dobrosavljević, D. Tanasković, M. Minakata, H. Fukazawa, and Y. Maeno, Phys. Rev. Lett. **93**, 146401 (2004).

[40] T. Ma, L. Zhang, C.-C. Chang, H.-H. Hung, and R. T. Scalettar, Phys. Rev. Lett. **120**, 116601 (2018).

[41] M. Pinterić, M. Čulo, O. Milat, M. Basletić, B. Korin-Hamzić, E. Tafra, A. Hamzić, T. Ivek, T. Peterseim, K. Miyagawa, K. Kanoda, J. A. Schlueter, M. Dressel, and S. Tomić, Phys. Rev. B **90**, 195139 (2014).

[42] M. Pinterić, P. Lazić, A. Pustogow, T. Ivek, M. Kuveždić, O. Milat, B. Gumhalter, M. Basletić, M. Čulo, B. Korin-Hamzić, A. Löhle, R. Hübner, M. Sanz Alonso, T. Hiramatsu, Y. Yoshida, G. Saito, M. Dressel, and S. Tomić, Phys. Rev. B **94**, 161105(R) (2016).

[43] T. Mori, Chem. Rev. **104**, 4947 (2004).